Journal of Molecular Catalysis A: Chemical (In Press, Available online 21 Oct 2013) Pre-Print

Acetaldehyde adsorption and condensation on anatase TiO_2: Influence of acetaldehyde dimerization

B. I. Stefanov, Z. Topalian, C. G. Granqvist, L. Österlund*

Department of Engineering Sciences, The Ångström Laboratory,
Uppsala University, P.O. Box 534, SE-751 21 Uppsala, Sweden

Abstract

Conversion of acetaldehyde to crotonaldehyde on anatase TiO_2 films was studied by in situ Fourier transform infrared spectroscopy (FTIR) and by density functional theory (DFT) calculations. In situ FTIR showed that acetaldehyde adsorption is accompanied by the appearance of a hitherto non-assigned absorption band at 1643 cm^{-1}, which is shown to be due to acetaldehyde dimers. The results were supported by DFT calculations. Vibrational frequencies calculated within a partially relaxed cluster model for molecular acetaldehyde and its dimer, and for the corresponding adsorbed species on the anatase (101) surface, were in good agreement with experimental results. A kinetic model was constructed based on the combined FTIR and DFT results, and was shown to explain the essential features of the acetaldehyde condensation reaction.

Keywords: TiO_2, acetaldehyde, crotonaldehyde, dimer, adsorption, DFT, FTIR

* Corresponding author: lars.osterlund@angstrom.uu.se

1. Introduction

Formaldehyde and acetaldehyde are two of the major indoor air pollutants and are released by many sources such as synthetic materials, building insulation, and domestic chemistry [1,2]. Accumulation of these volatile organic compounds (VOCs) may be enhanced through inadequate techniques for ventilation and air conditioning [3]. The present study considers acetaldehyde, which is a well-known potential human carcinogen [4] for which maximum occupational exposure levels are set in Europe and the USA [5,6]. Several methods have been suggested to improve the indoor air climate, and among them TiO_2-based photocatalysis has been recognized as a sustainable and environmentally friendly alternative for indoor VOC abatement, yielding only CO_2, H_2O, and trace mineral acids as reaction products with only low-power UV light as external energy source [7,8]. Photo-oxidation of acetaldehyde on TiO_2 has been the subject of several studies [9–11], and has also been proposed as a model compound for estimating the activity of photocatalytic materials for air purification [16]. It is therefore of utmost importance to have a comprehensive understanding of the elementary photo-oxidation steps of acetaldehyde on TiO_2.

There are a number of detailed studies of the oxidation of aldehydes, including of acetaldehyde, in the literature [12–21]. These investigations are relevant also for the photo-oxidation other VOCs, since acetaldehyde can be an intermediate in those reactions, as is the case e.g. for photo-oxidation of acetone [13] and ethanol [14]. Major intermediate acetaldehyde oxidation products include formate, acetic acid, and formaldehyde [12–16]. Furthermore, it is recognised that at room temperature—even without irradiation—adsorption of acetaldehyde on TiO_2 is accompanied by condensation to form crotonaldehyde [17], with 3-hydroxybutanal being a short-lived intermediate [18]. Similar condensation reactions are known to occur also on other oxide surfaces such as CeO_2 [19], ZrO_2, MgO [20] and Al_2O_3 [21]. Crotonaldehyde converts into other surface species in the acetaldehyde oxidation pathway. In many applications it is desirable to suppress formation of species with higher mass, such as in photocatalytic air cleaning. It has been recognized that condensation can be suppressed by supporting the catalyst on a noble metal support [22], or increasing the surface acidity through SO_4 modification [31].

In the present study we explore the molecular steps involved in the condensation reaction for acetaldehyde on anatase TiO_2 nanoparticles, which mainly expose their (101) surfaces, by using an

interplay between in situ Fourier transform infrared spectroscopy (FTIR) and density functional theory (DFT) calculations. In addition, we explore another property of acetaldehyde, which seldom has been recognized in the past: viz., its ability to form hydrogen-bonded complexes in the gas phase and thereby influence the adsorption kinetics. Thus we investigate the possibility of co-adsorption of acetaldehyde monomers and hydrogen-bonded acetaldehyde dimers, and its implications for the observed surface reaction kinetics. A textbook example of such interactions is the dimerization of acetic acid vapours, wherein the dimers are stable even at elevated temperature [23], and similar behaviour was observed for acetaldehyde already in the mid-1930s when Milverton demonstrated that the thermal conductivity of acetaldehyde in gas phase increased with increasing gas pressure [24]. Alexander and Lambert measured the second virial coefficient for acetaldehyde and observed a significant deviation from the value obtained from the Berthelot equation [25], and concluded that the extra interaction was due to the formation of cyclic dimers. Later Wilkinson and co-workers contributed to the topic in the 1940s with similar measurements, as well as by providing a theoretical explanation for the mentioned behaviour of acetaldehyde and other polar gases [26]. Just a few recent studies have reported on acetaldehyde dimerization [27–30], and the only experimental data known to us is the study by Curtiss and Blander, who also calculated the enthalpy of dimerization for a number of hydrogen-bond-forming compounds, including acetaldehyde [27]. They used results from the literature for the deviation from the ideal gas behaviour of vapour phase thermodynamic data. Hermida-Ramón and Ríos performed first-principles calculations on a series of possible structures of acetaldehyde dimers and elucidated the most stable geometry [30], which they reported to be one of the least symmetric structures.

2. Experimental

2.1 Materials

Commercially available anatase TiO_2 nanoparticles (DSL 18NR-T, DyeSol Ltd., Queanbeyan, Australia) were used to prepare films by the doctor-blading technique on infrared-transparent CaF_2 substrates (Crystran Ltd., Pole, UK). After coating, the samples were left to dry overnight, and were subsequently sintered at 500 $^{\circ}$C for 1 h prior to use. A more detailed characterisation of TiO_2 films prepared in this manner has been presented elsewhere [31].

2.2 Materials characterization

Grazing-incidence X-ray diffraction (GIXRD) was performed with a Siemens D5000 diffractometer using CuK_α radiation with 1° incident angle (Figure 1). It is evident from the GIXRD results that the films contained only the anatase phase. The mean crystallite size D was estimated from Scherrer's formula, $D = K\lambda/(\beta cos\theta_d)$, where K is a dimensionless constant (here assumed to be 0.9, which is appropriate for spherical grains), $2\theta_d$ is the diffraction angle, λ is the X-ray wavelength (1.5406 Å), and β is the full width at half-maximum of the diffraction peak. The mean crystallite size was D = 11.5 nm, as determined from the strongest diffraction peak (the <101> reflection).

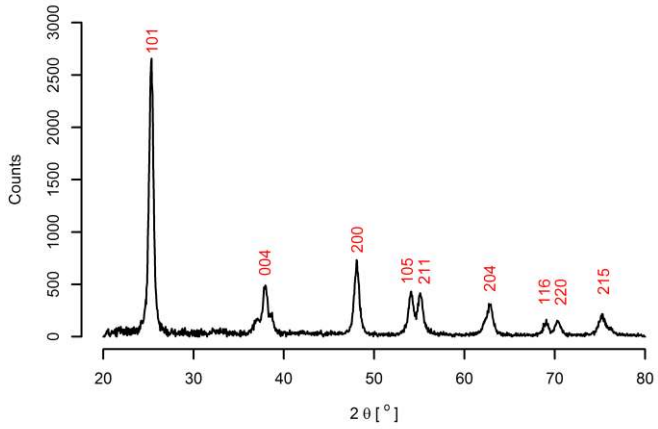

Figure 1 X-ray diffractogram of a TiO_2 film showing a pure anatase phase.

Transmission electron microscopy (TEM) measurements were performed with a JEOL 2000 FX II microscope operated at an accelerating voltage of 200 kV. TEM samples were prepared by suspending a small amount (< 1 μg) of TiO_2 in 5 ml of acetone and subsequent sonication (35 kHz) for 15 minutes. A TEM grid (400 mesh holey carbon film, Agar Scientific, Stansted, UK) was dipped into the suspension and dried in air. The particles were found to have a truncated tetragonal pyramidal shape, in good agreement with the Wulff polyhedron for anatase exposing mainly its minimum surface energy (101) facets (Figure 2). Distinct fringes separated by 3.5 Å were observed in the TEM images, which corresponds to the inter-planar spacing of anatase in the [101] direction (Figure 2d), and shows that the particles have predominantly (101) facets.

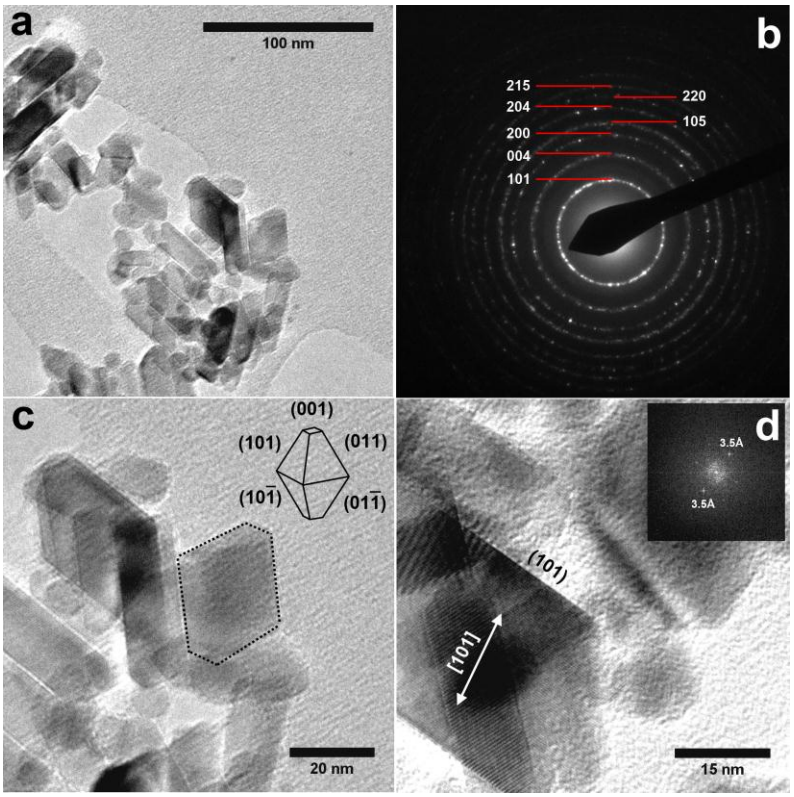

Figure 2 (a) Representative TEM images of anatase TiO_2 nanoparticles; (b) selected-area electron diffraction pattern obtained from the image shown in panel (a), and showing the expected diffraction rings due to TiO_2; (c) high-magnification image of the particles in panel (a) demonstrating the truncated tetragonal bipyramidal shape of the nanoparticles and the corresponding Wulff reconstruction of the anatase particles (inset); and (d) atom-resolved lattice fringes showing the inter-planar spacing along the [101] direction.

2.3 In situ FTIR spectroscopy

Acetaldehyde adsorption was investigated by in situ Fourier-transform infrared (FTIR) spectroscopy, using a vacuum-pumped FTIR spectrometer (Bruker IFS66v/S, Ettlingen, Germany) equipped with a modified IR transmission reaction cell, as described elsewhere and schematically depicted in Figure 3 [32,33]. The IR reaction cell was connected to a home-made gas flow system with a set of computer-controlled mass flow regulators. The gas flow was set at 100 ml min^{-1}, employing synthetic air (20 % O_2 and 80 % N_2 with purities 99.999 % and 99.994 %, respectively), and acetaldehyde (90 ppm CH_3CHO with purity in N_2 with 99.999% purity). The acetaldehyde gas phase concentration was set to 50 ppm in the experiments.

Repeated FTIR spectra were acquired with 2 cm^{-1} resolution once per minute, corresponding to

150 co-added spectra at a forward/reverse scan rate of 20 Hz. Details about the acquisition procedure can be found elsewhere [31]. The spectra were baseline-corrected and transferred to the R program environment for further analysis [34].

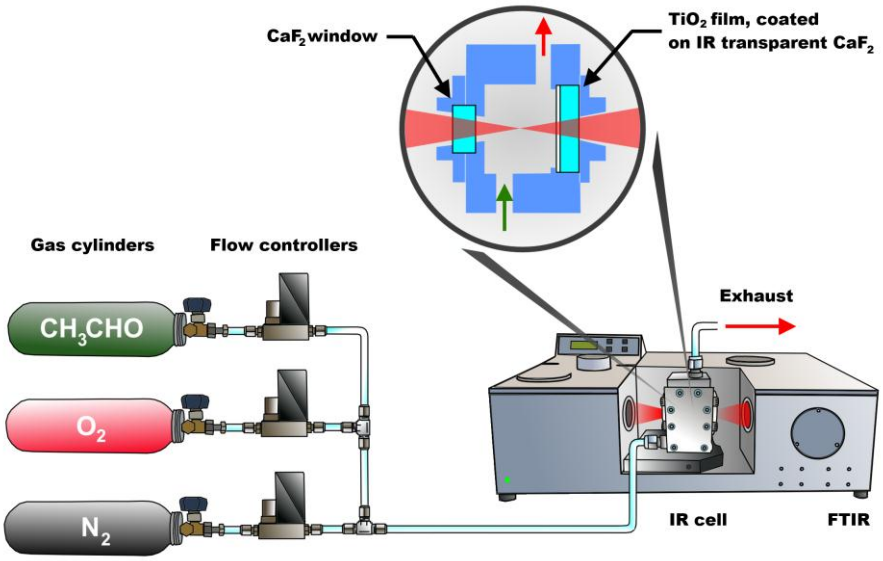

Figure 3 Schematic picture of the in situ FTIR set-up used for studying acetaldehyde adsorption on TiO_2.

A permanently aligned 8-meter-pathlength gas cell (Infrared Analysis, Inc., Anaheim, USA) was used to obtain gas-phase IR spectra of acetaldehyde. The spectra were obtained with the same spectrometer settings as in the FTIR surface analysis measurements, after saturation of the cell with 50 ppm acetaldehyde in nitrogen.

2.4 DFT calculations

Density functional theory (DFT) calculations were performed with the GAMESS quantum-chemical package, version 11 AUG 2011 (R1) [35], employing the M06 hybrid meta-functional developed by Truhlar and co-workers, which is known to give good results for non-covalent interactions [36,37].

A saturated cluster model with the formula $Ti_5O_{18}H_{16}$ was used to represent the dominant anatase (101) surface. The structure of the cluster is shown in Figure 4, and is based on crystallographic data for the anatase unit cell at 25 °C [38]. Geometric optimization was done with the cluster partially relaxed—with the peripheral oxygen and the saturation hydrogen atoms fixed—to provide stability for the structure. The spacing in the [010] direction changed from 3.78 Å to 3.80 Å during the relaxation.

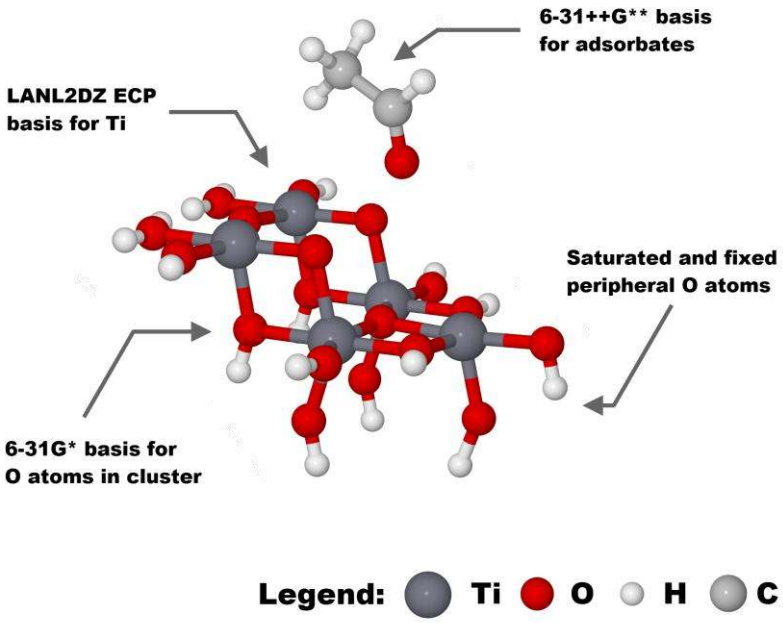

Figure 4 Structure of the $Ti_5O_{18}H_{16}$ cluster model used to represent the anatase (101) surface in the DFT calculation, and the acetaldehyde molecule prior to geometry optimization. The basis sets used for geometry optimization of the structure at different levels are indicated.

The equilibrium geometry of the adsorbate–cluster system was calculated in several steps. First, a rough optimization was performed with minimal basis sets employing the Huzinaga MIDI basis sets [39]. The resulting geometry was then re-optimized by use of a combination of basis set functions: the LANL2DZ ECP basis [40] was employed for the Ti atoms in the cluster, as obtained from the Basis Set Exchange (BSE) database [41], and the standard Pople split-valence 6-31G* basis set was used for cluster oxygen and hydrogen atoms. Finally, the 6-31++G** basis set was used for the adsorbate [42–44]. The adsorption structure was derived by positioning the optimized adsorbate geometry over the

relaxed cluster with the C=O group oriented toward the 5-fold coordinated Ti^{4+} centre. The distance between the adsorbate and the cluster was 5 Å. The energy was then minimized, first with the lower basis sets (MIDI) and then by re-optimization at the higher levels (LANL2DZ/6-31G/6-31++G**).

Several types of data were extracted from the calculations: the total electronic energy, the zero-point energy correction to the electronic energy (ZPE), the Gibbs free-energy correction to the total electronic energy (*G*), the entropy correction to the total electronic energy (*S*), and the IR vibrational frequencies. All electronic energies were counterpoise (CP) corrected using the Boys and Bernardi scheme [45]. The binding energy between the adsorbate and the cluster was calculated as

$$\Delta E = E(Adsorbate@Cluster) - E(Cluster) - E(Adsorbate), \quad (1)$$

where ΔE is the energy change due to the adsorption, and E are CP- and ZPE-corrected total electronic energies. The adsorption enthalpy ΔH and free energy change ΔG were computed in a similar way, but, instead of using a ZPE-correction, the total electronic energies of each of the interacting species were adjusted with the thermal correction to standard conditions (298.15 K, 1 atm) and with the Gibbs free-energy correction, as calculated by GAMESS (which includes the ZPE).

The IR vibrational frequencies were computed at the high computational level by means of the default two-point method in GAMESS, and were corrected with a scaling factor of 0.947, as recommended by the National Institute of Standards and Technology (NIST) [46]. Derivatives of the vibrational spectra—such as ZPE, entropy, thermal and free-energy corrections—were also scaled with the same factor. To compare with the experimental data, the IR spectra were plotted after convoluting the calculated frequencies with Lorentzian functions using a home-made R script.

3. Results and discussion

3.1 Acetaldehyde adsorption

The adsorption experiments were divided into two parts: First, the sample was dosed with 50 ppm acetaldehyde in synthetic air for a duration t = 12 minutes and, then the reaction cell was purged with synthetic air for t = 10 minutes. Figure 5 shows representative IR spectra acquired during gas dosing, at saturation coverage, and at the end of the purging period.

Strong absorption bands at 1693 cm^{-1} and 1130 cm^{-1} appeared in the FTIR spectra during gas dosing (Figure 5a). They are due to the ν(C=O) and ν(C–C) modes of acetaldehyde, respectively [18]. The large red-shift of the carbonyl vibration, compared to the gas-phase value of 1760 cm^{-1}, indicates that the acetaldehyde is coordinated with a surface site through the carbonyl oxygen, as in –C=O → Ti^{4+} [47]. In addition, other absorption bands appear at 1643 cm^{-1} and 1674 cm^{-1}, and weaker bands are noted at 1355 cm^{-1} and 1375 cm^{-1}. The former two peaks have previously been assigned to the δ(CH) and $\delta_s(CH_3)$ modes in acetaldehyde [48]. However, as we demonstrate below, the assignment of the weaker bands in the carbonyl region between 1640 cm^{-1} and 1680 cm^{-1} is non-trivial.

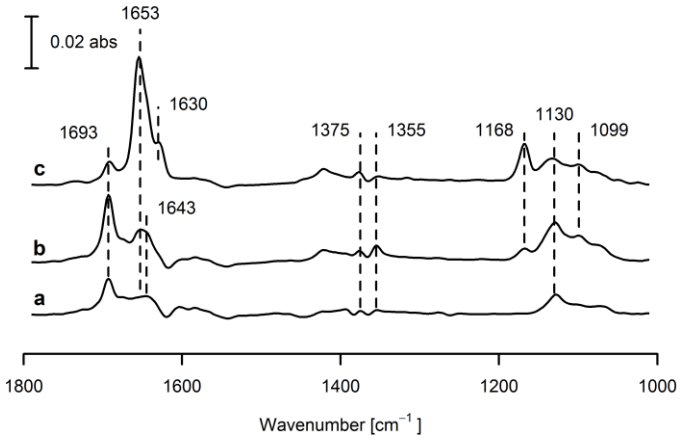

Figure 5 IR spectra recorded during exposure of TiO_2 to acetaldehyde. (a) during acetaldehyde adsorption at t = 6 minutes; (b) after saturation with acetaldehyde at t = 13 minutes; and (c) after purging the reaction cell in synthetic air at t = 22 minutes, when conversion to crotonaldehyde is observed. The frequencies corresponding to the main features of both compounds are marked, as is the broad peak at 1643 cm^{-1} appearing during the initial phase of dosing.

With increasing acetaldehyde coverage a new band develops at 1653 cm^{-1}, which eventually becomes stronger than the peak at 1643 cm^{-1}. The evolution of this process is shown in Figure 6(a)–(c), where the contribution of the various carbonyl bands has been deconvoluted. Simultaneously, new peaks appear at 1168 cm^{-1} and 1099 cm^{-1} (Figure 5b). The features at 1653 cm^{-1} and 1168 cm^{-1} are consistent with the ν(C=O) and ν(C–C) modes due to crotonaldehyde, respectively, and indicate that condensation of acetaldehyde takes place [18]. During purging, the peaks at 1693 cm^{-1} and 1130 cm^{-1} decrease, and simultaneously the intensity of the peaks at 1653 cm^{-1} and 1168 cm^{-1} increase, signalling

almost complete conversion of acetaldehyde to crotonaldehyde (Figure 5c). A less intense band also develops at 1630 cm^{-1}; it is associated with the ν(C=C) vibration of crotonaldehyde [49].

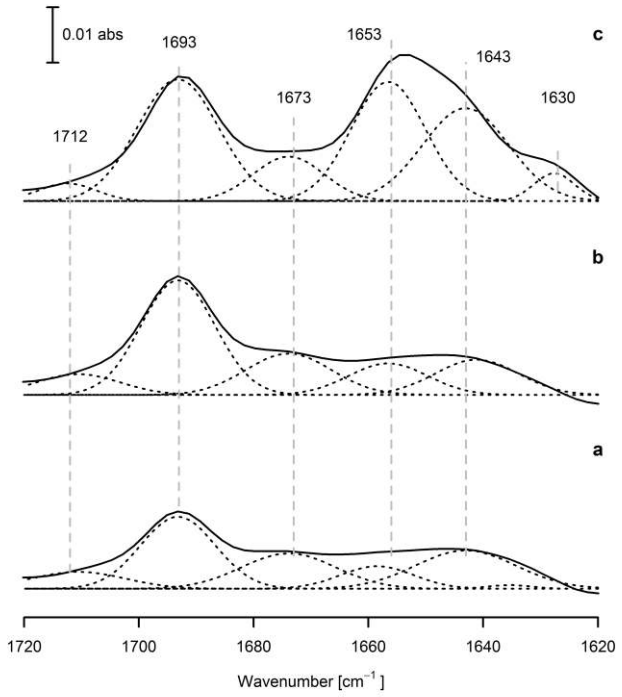

Figure 6 Deconvolution of absorption bands in the carbonyl vibration region, using Gaussian functions, for data recorded during exposure of TiO_2 to acetaldehyde. (a) during acetaldehyde adsorption, at t = 6 minutes, where the 1643 cm^{-1} peak reaches is maximum; (b) at a later time, with t = 9 minutes, where the 1643 cm^{-1} peak has decreased slightly; and (c) during the conversion of acetaldehyde to crotonaldehyde, at t = 15 minutes, where the 1643 cm^{-1} peak has merged with the crotonaldehyde carbonyl peak.

The kinetics of acetaldehyde adsorption and its condensation to crotonaldehyde were investigated. Quantitative data were extracted from the IR spectra by using integrated areas of the carbonyl peaks for acetaldehyde and crotonaldehyde, as indicated in Figure 7(a). The following integration ranges were used: 1708 – 1680 cm^{-1} for acetaldehyde, and 1668 – 1630 cm^{-1} for crotonaldehyde. With these choices of integration ranges the influence of variations of surface water bands in the 1615-1620 cm^{-1} is avoided. The conversion of the FTIR absorbance to coverage was done

in two steps [31]. First, the maximum coverage for both species was determined. For acetaldehyde this was done by fitting the absorbance data with the analytical solution appropriate for a Langmuir isotherm according to

$$A(t) = A^{sat}(1 - e^{-k^{ad}t}), \qquad (2)$$

where A is the measured absorbance, and k^{ad} is rate of adsorption. The data for acetaldehyde was normalized by the saturation absorbance A^{sat}. The surface coverage θ is then defined as $\theta(t) = A(t)/A^{sat}$. The data for crotonaldehyde was normalized to its observed maximum coverage, and scaled by a factor of ½ to ensure stoichiometry, since we expect a complete conversion on the TiO_2 surface, where the maximum observed coverage for crotonaldehyde should be half of the acetaldehydes. This approach worked satisfactory well, as seen by the normalized traces of selected absorption bands shown in Figure 7(b). Even though none of the species were scaled to its IR absorption cross-section prior the normalization, the coverage of crotonaldehyde at the end of the condensation cycle was approximately half of the amount of adsorbed acetaldehyde. This success is however deceptive, and disguises the fact that the intermediate crotonaldehyde and dimer concentrations cannot be resolved with confidence, since they are treated simultaneously in the fitting procedure. The error introduced in this way should however not be too large. First, considering the stoichiometry of the dimer → acetaldehyde → crotonaldehyde reaction, which is 1 : 2 : 1. This implies that both the normalized dimer and crotonaldehyde coverage should be scaled with ½ with respect to acetaldehyde. Second, the cross-sections for both crotonaldehyde and the dimer should be approximately twice that of acetaldehyde. The largest error introduced by treating the crotonaldehyde and the dimer bands together comes instead from the fact that the information for the maximum coverage of the dimer is lost. Only the ratio between the dimer and crotonaldehyde is preserved. This introduces errors in the rate constants we obtain.

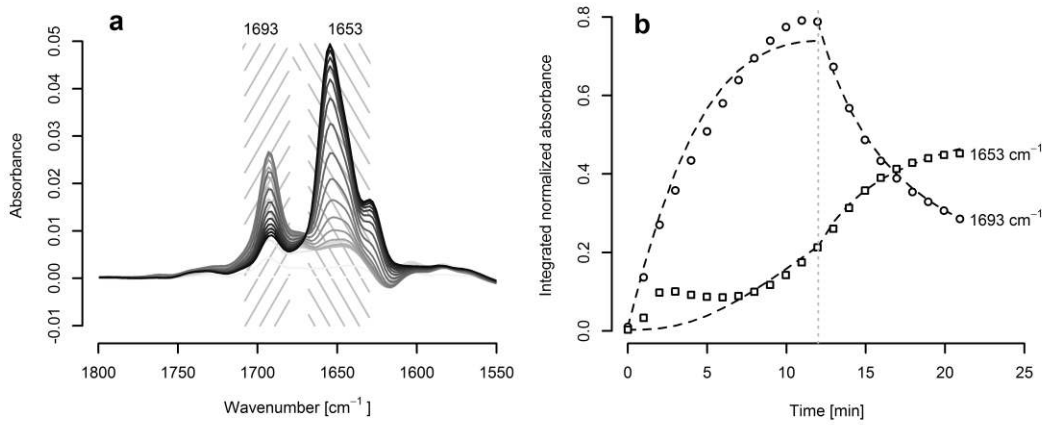

Figure 7 (a) Progression of carbonyl peaks for acetaldehyde (1693 cm^{-1}) and crotonaldehyde (1653 cm^{-1}) during gas-phase exposure of TiO_2 to acetaldehyde. The integration range used to quantify the peak areas are indicated by the hatched rectangular areas. (b) Time-traces of the integrated carbonyl bands for acetaldehyde and crotonaldehyde as a function of time (gas dosing at $0 < t < 12$ minutes; purging in synthetic air at $13 < t < 23$ minutes); dashed curves indicate results from the simplified kinetic model, which fail to account for the contribution of the intermediate species, which appear between $0 < t < 5$ minutes (see main text).

To fit the integrated IR absorption data, a kinetic model was constructed based on the observed acetaldehyde adsorption and condensation reactions according to

$$2CH_3CHO_{gas} \rightarrow 2CH_3CHO_{ads} \rightarrow CH_3(CH)_2CHO_{ads} + H_2O\,. \qquad (3)$$

The condensation reaction is second order, which leads to the following set of rate equations to describe the dosing part of the experiment:

$$\frac{d\theta_A}{dt} = k_A^{ad}(1.5 - \theta_A - \theta_C) - k_A^{cond}\theta_A^2\,, \qquad (4)$$

$$\frac{d\theta_C}{dt} = \frac{1}{2}k_A^{cond}\theta_A^2\,, \qquad (5)$$

where k_A^{ad} and k_A^{cond} are rate constants for acetaldehyde adsorption and condensation, respectively, and θ_A and θ_C are surface coverages for acetaldehyde and crotonaldehyde, respectively. The prefactor ½ in

Eqn. (5) accounts for the stoichiometry. It should be noted that the factor $(1.5-\theta_A-\theta_C)$ in Eqn. (4) yields a maximum number of sites equal to 1.5 instead of 1; this follows from a normalization artefact due to independent estimates for the saturation coverage of acetaldehyde and crotonaldehyde. The integrated spectral data for acetaldehyde is normalized to its predicted saturation coverage using the initial adsorption data employing Eqn. (2). Thus we neglect the fact that crotonaldehyde is formed during acetaldehyde adsorption, which in its turn occupies available sites. Moreover, the data for crotonaldehyde are integrated over a different spectral region than that for acetaldehyde and has its own normalization. Crotonaldehyde is not an adsorbing species in reaction (3), and therefore its final coverage is linked through stoichiometry to the coverage of acetaldehyde by a factor ½, assuming that they occupy the same sites (this assertion is rationalized in Sec. 3.2 below). Thus even though acetaldehyde and crotonaldehyde occupy the same sites, their total saturation coverage would not be 1, but instead 1.5 employing our absorbance normalization method; hence the term $(1.5-\theta_A-\theta_C)$.

Figure 7(b) shows experimental data and results of the kinetic model for acetaldehyde adsorption and condensation reactions represented by Eqs. (4) and (5). The fitting was done in two parts: one for gas dosing, and one for purging. The difference between the two models is the rate of acetaldehyde adsorption, which of course is zero during purging. It is evident that, during gas adsorption, the fit does not describe the data correctly during the first 6 minutes. The reason for this can be traced to the existence of several carbonyl bands (see Figure 6) contributing to the integrated absorbance of the crotonaldehyde band (at 1653 cm^{-1} in Figure 7b). The appearance and time-dependence of these bands are independent of spectral pre-processing, integration method, and peak-deconvolution scheme, which demonstrates that they are robust spectral features.

The failure to model the time-dependence of the spectral features in Figure 7(b) by Eqn. (5) suggests that the pertinent absorption bands are not caused by the condensation reaction. On the other hand, the fact that the absorption peak at 1643 cm^{-1} occurs simultaneously with the features of adsorbed acetaldehyde indicates that it is associated with a co-adsorbing species. To investigate this possibility, we analysed the time-dependence of the deconvoluted peak areas (Figu 8). First one notices that the evolution of the weak peaks at 1712 cm^{-1} and 1673 cm^{-1} is consistent with an increase of acetaldehyde coverage (see Figure 6). Their proximity to the main acetaldehyde peak at 1693 cm^{-1} may suggest differently coordinated acetaldehyde molecules, probably related to non-reactive sites. We tentatively associate the peak at 1673 cm^{-1} with a CH_3CHO molecule bonded between two Ti^{4+} centres, on edges, or on an oxygen vacancy site, while the peak at 1712 cm^{-1} may be related to weaker binding

sites, such as hydroxyl groups or adsorbed water molecules. The intensity of the peaks at 1643, 1693 and 1673 cm^{-1} increases at the same rate during the first minutes of adsorption, which indicates that all of them are related to acetaldehyde. However after 6 minutes of gas dosing, the peak at 1643 cm^{-1} decreases despite the fact that the acetaldehyde coverage increases. It should be noted that the results from the deconvolution show a slight shift by about 2 cm^{-1} of this peak during the first 3 minutes of gas dosing. The progression of this peak between 6 and 10 minutes becomes uncertain when the crotonaldehyde coverage increases, which is due to its proximity to the ν(C=O) and ν(C=C) peaks located at 1653 cm^{-1} and 1630 cm^{-1}, respectively. At t > 10 minutes, an absorption peak appears at 1643 cm^{-1} and increases at the same rate as the crotonaldehyde absorption; therefore it can be tentatively attributed to differently coordinated crotonaldehyde species. Hence two overlapping spectral bands exist at t > 10 min.

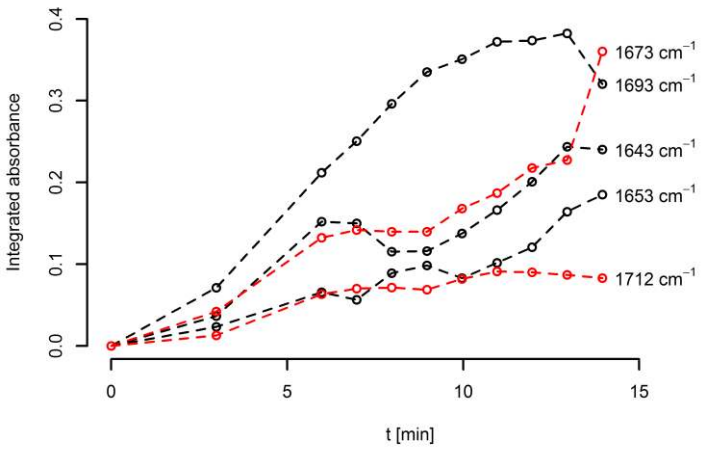

Figure 8 Time-traces of deconvoluted FTIR bands during exposure of TiO_2 to acetaldehyde.

Below we focus on the species responsible for the deviating kinetics apparent during the first 6 minutes of acetaldehyde adsorption. A reasonable hypothesis based on the spectral and kinetic data presented in this section, as well as the known properties of aldehyde dimers discussed in the Introduction, is that the peak at 1643 cm^{-1} is due to acetaldehyde dimers. The existence of this species is further investigated in the following section.

3.2 DFT calculations

We performed DFT calculations in order to get further insights into acetaldehyde adsorption and reactions on the anatase (101) surface. Several model systems were investigated encompassing acetaldehyde, its dimer, and crotonaldehyde in gas phase, as well as the corresponding molecules adsorbed on an anatase (101) cluster surface. Water adsorption was also included in the models and was used as a reference for calculating the acetaldehyde → crotonaldehyde condensation energy on the surface.

For the acetaldehyde dimer itself there are several possible configurations for its structure in gas phase. We have considered seven structures taken from the work of Hermida-Ramón et al. [30].

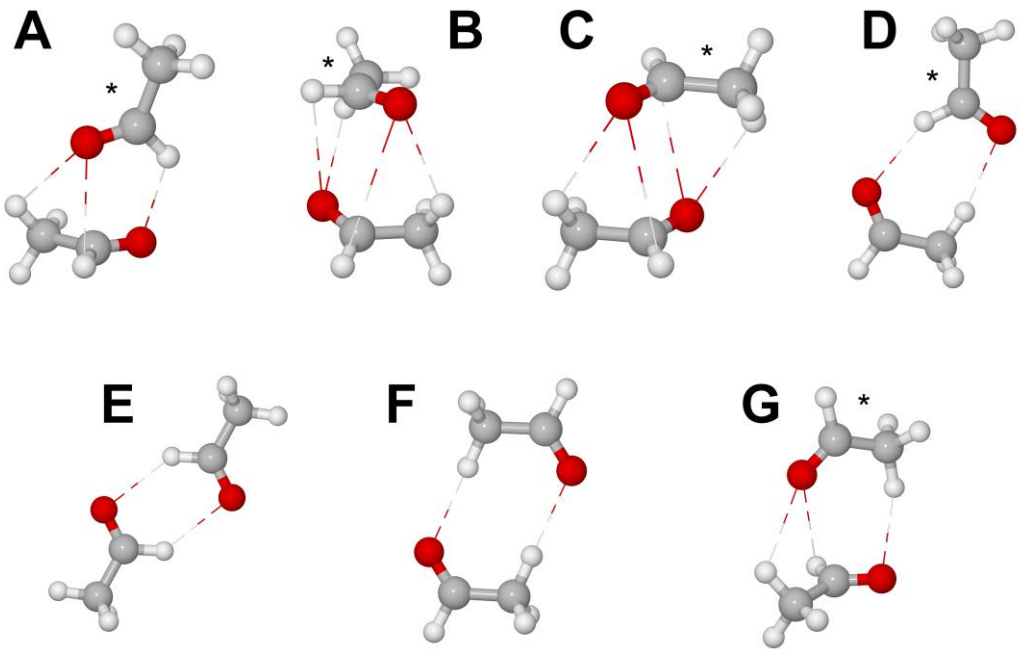

Figure 9. Optimized geometries for seven different dimer structures of acetaldehyde in gas phase. Structures taken from Ref. 30.

The structures are shown in Figure 9 and denoted by capital letters from A to G. The thermochemical data for dimerization of the structures are presented in Table 1. Geometric data about the seven gas phase species is summarized in Table 2. The least symmetric structure (denoted A in Figure 9), was found to be the most stable one and was chosen for the adsorption calculations.

Table 1 Calculated thermochemical data and predicted IR frequencies for the seven acetaldehyde dimer configurations shown in Figure 9.

Structure (Fig. 9)	ΔE, kJ mol^{-1}	ΔH^{298}, kJ mol^{-1}	ΔS, J mol^{-1} K^{-1}	ΔG^{298}, kJ mol^{-1}	ν(C=O)Calc, cm^{-1}
A	-16.40	-15.10	-117.08	19.80	1744.8
B	-15.90	-14.76	-119.68	20.93	1747.4
C	-14.76	-13.39	-117.29	21.58	1750.3
D	-11.91	-10.23	-109.88	22.54	1751.5
E	-11.18	-8.94	-99.11	20.61	1742.4
F	-11.16	-11.43	-127.48	26.58	1754.7
G	-14.18	-13.13	-120.37	22.76	1750.9

The structure, presented at Figure 10a has an advantage over the symmetric alternatives in that the carbonyl group is available for surface interactions. The dimerization energy was calculated to be ΔE = –16.4 kJ mol^{-1} and ΔH = –15.10 kJ mol^{-1}. This is in agreement with previously calculated values for this configuration (ΔE = –16.57 kJ mol^{-1}, obtained with MP2/6-311+G(2d,p)) [30]. It is also close to the experimental result ΔH = –16.4 kJ mol^{-1} reported by Curtiss and Blander [27].

Table 2. Geometric parameters and partial charges of the dimer structures shown in Figure 9

		CH_3CHO	Dimer						
			A	B	C	D	E	F	G
r(C - O)		1.206	1.213	1.212	1.212	1.212	1.213	1.211	1.212
	*		1.213	1.212	1.212	1.214	1.213	1.211	1.212
r(C H)		1.117	1.113	1.115	1.115	1.116	1.113	1.116	1.114
	*		1.114	1.114	1.115	1.114	1.114	1.116	1.115
r(O···H)			2.326	2.890 2.738	2.559 3.479	2.346	2.399	2.345	2.435
	*		2.809 2.735	2.482 3.810	2.580 3.396	2.333	2.397	2.345	2.643 2.792
q(O)		-0.382	-0.413	-0.414	-0.404	-0.387	-0.404	-0.394	-0.397
	*		-0.413	-0.404	-0.404	-0.390	-0.403	-0.394	-0.413
q(C)		0.249	0.345	0.299	0.280	0.224	0.428	0.281	0.319
	*		0.420	0.285	0.286	0.424	0.432	0.279	0.292

(*) Data for the non-symmetric monomer unit shown with asterisks in Fig. 9. All distances in Å. Partial charges are based on Mulliken population analysis.

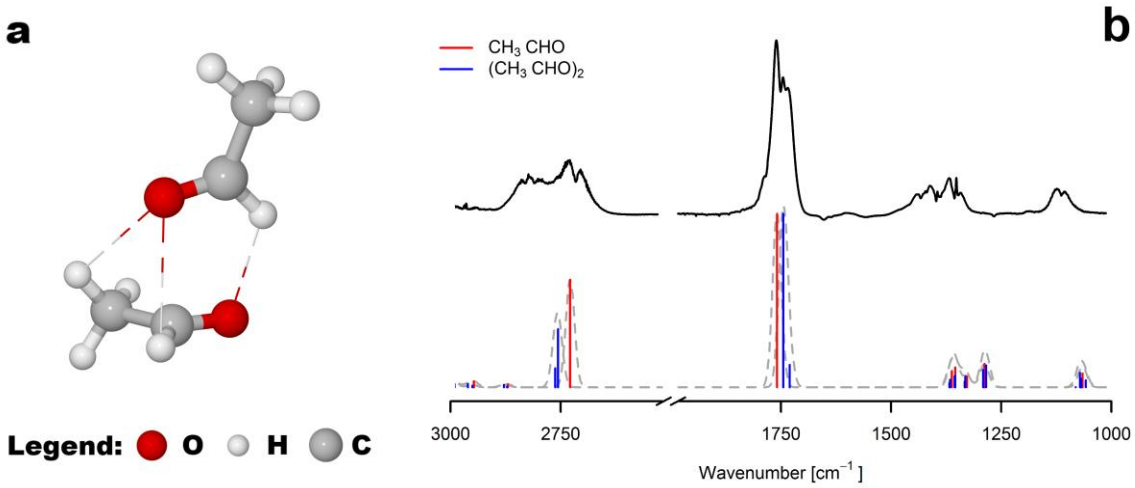

Figure 10 (a) Optimized geometry of the most stable acetaldehyde dimer configuration according to DFT calculations. (b) Comparison between observed acetaldehyde gas phase FTIR spectra and predicted vibrational frequencies for acetaldehyde and its dimer; the computed spectra were convoluted with Lorentzian functions to obtain the dashed curves.

The Gibbs free energy of dimerization ΔG was also calculated, but it must be emphasized this value is provided only for comparison since it is related to the computed entropy of the transition ΔS, which is uncertain (and calculated for the isolated dimer in vacuum). Even with this approximations in mind for the dimerization process, the predicted value ΔG = 19.8 kJ mol^{-1} suggests a monomer–dimer equilibrium, which under standard conditions should be shifted towards the free monomer (K^{dim} = 3.38 × 10^{-4}). However, we can expect that, in the gas phase, the acetaldehyde will have lower entropy than that of the isolated molecule due to intermolecular interaction, and hence ΔS of dimerization will be smaller, thus favouring dimerization.

Figure 10(b) shows calculated IR spectra of acetaldehyde together with an experimental spectrum measured for 90 ppm of acetaldehyde in nitrogen. According to the calculations, the dimerization causes a red-shift of 14 cm^{-1} for the ν(C=O) band. Deconvolution of the main carbonyl peak of the experimental spectra shows several red-shifted peaks, consistent with the existence of dimers.

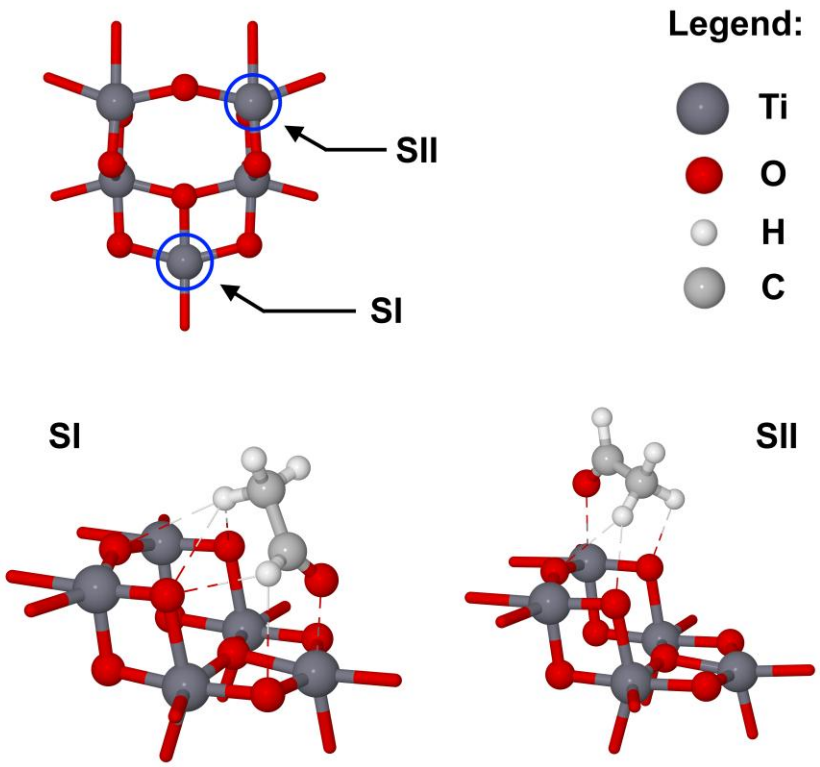

Figure 11 The two symmetrically unique adsorption sites SI and SII on the (101) cluster model, along with the optimized structures for adsorbed acetaldehyde.

In the $Ti_5O_{18}H_{16}$ cluster model there were two exposed Ti centres, which act as Lewis sites and coordinate with the C=O group of the adsorbing acetaldehyde. They are denoted SI and SII in Figure 11. For the acetaldehyde model two calculations were done, each preceded by geometry optimization of the approaching adsorbate towards each site. The resulting geometries are also shown in Figure 11. They differ by the number of hydrogen bonds formed between the cluster and the adsorbed acetaldehyde molecule. In the SI configuration five hydrogen bonds form, while three bonds form in

the SII configuration. Vibrational frequencies and thermochemical quantities were calculated for both structures. SI yielded an adsorption energy of ΔE = –79.79 kJ mol^{-1}, while for SII it was slightly lower with ΔE = -75.63 kJ mol^{-1}, confirming that the adsorption energy is dominated by the C=O → Ti interaction. Both structures yielded similar vibrational frequency of the ν(C=O) mode (1690 cm^{-1} for SI, and 1693 cm^{-1} for SII). The latter is in perfect agreement with the experimental value. Despite this we nevertheless chose to use the SI site for the subsequent adsorption calculations, since this yielded the lower energy structure.

Table 3 Calculated thermochemical data and predicted IR frequencies for acetaldehyde–TiO_2 surface reactions at room temperature. Experimental frequencies are included for comparison. A denotes monomer acetaldehyde, D denotes dimer, and C crotonaldehyde.

Reaction	Calculated thermochemistry				IR frequencies*	
	ΔE, kJ mol^{-1}	ΔH, kJ mol^{-1}	ΔS, J mol^{-1} K^{-1}	ΔG, kJ mol^{-1}	ν(C=O)^{Calc}, cm^{-1}	ν(C=O)^{Exp}, cm^{-1}
2A → D	-16.4	-15.1	-117.08	19.8	1759 → 1745	1760 → 1745, 1734
A + TiO_2 → A-TiO_2	-79.79	-80.73	-180.62	-26.88	1759 → 1690	1760 → 1693
D + TiO_2 → D-TiO_2	-77.85	-79.82	-222.79	-13.4	1745 → 1653	1745 → 1643
D-TiO_2 + TiO_2 → 2A-TiO_2	-65.33	-66.52	-21.36	-60.16	1653 → 1690	1643 → 1693
D-TiO_2 → A-TiO_2 + A	14.46	14.2	389.75	-33.28	1653 → 1690, 1759	1643 → 1693
2A-TiO_2 → C-TiO_2 + H_2O-TiO_2	-9.24	-10.49	-9.06	-7.79	1690 → 1660	1693 → 1653

(*) Values indicate vibrational frequencies for (gas phase state) → (adsorbate state).

Figure 12 depicts the structures resulting after adsorption of the optimized acetaldehyde molecule and its dimer on the anatase (101) surface. As discussed above the adsorption energy for the acetaldehyde was calculated to be ΔE = –79.79 kJ mol^{-1}. For the dimer it is only slightly lower, ΔE = –77.85 kJ mol^{-1}. The similarity between the two values can be explained by the related adsorption geometry of the interacting acetaldehyde molecules, and the equal number of bonds formed with the surface (which was also the basis for our assumptions regarding site occupancy in Sec. 3.1). However since the dimer has lower entropy per acetaldehyde unit than free acetaldehyde, there is a significant difference in ΔG; it is a factor of two smaller for the dimer adsorbate structure. The ν(C=O) vibration of

the adsorbed acetaldehyde was calculated to be at 1690 cm^{-1}, which is in good agreement with the experimental value. For the adsorbed dimer, the ν(C=O) frequency of the interacting molecule is down-shifted to 1653 cm^{-1}, which agrees well with the measured frequency 1642 cm^{-1} observed during the initial adsorption period according to Figures 7 and 8.

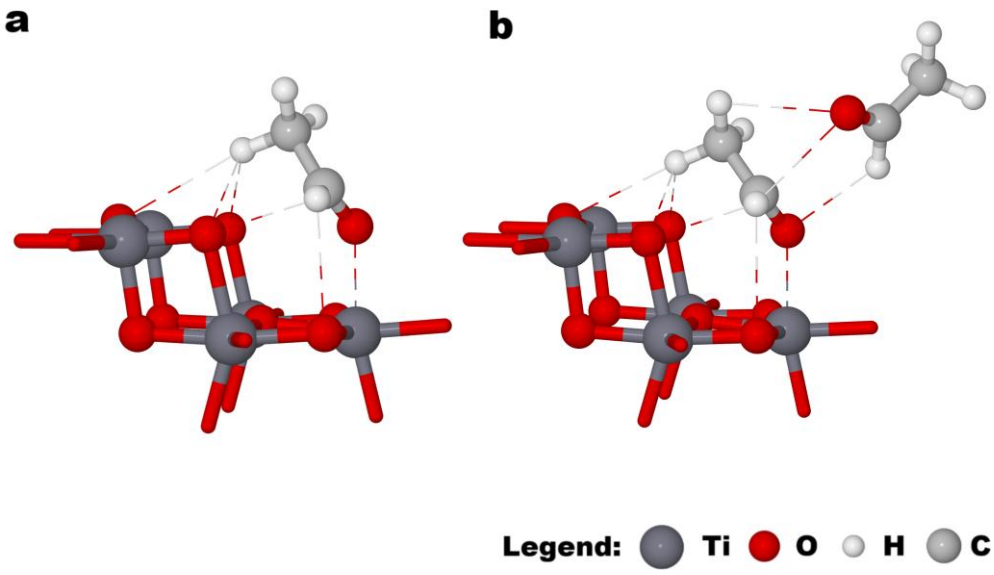

Figure 12. (a) Calculated equilibrium structures of acetaldehyde, and (b) of its dimer, adsorbed on the anatase (101) surface of a $Ti_5O_{18}H_{16}$ cluster.

It is clear that entropic reasons predict that adsorbed dimers will be less energetically feasible than adsorbed acetaldehyde. We can then assume the following scenario for the dimer's fate on the surface: First, it may decompose with release of a free acetaldehyde molecule into the gas phase by

$$D-TiO_2 \rightarrow A-TiO_2+A \quad . \qquad (6)$$

Our calculations show that this reaction is not energetically favoured with regard to enthalpy (ΔE = 14.46 kJ mol^{-1}), but the reaction could be feasible for entropic reasons (ΔS = –389.75 J mol^{-1} K^{-1}; ΔG = –33.28 kJ mol^{-1}). The second possible pathway requires availability of an extra adsorption site for acetaldehyde; in this case the dimer may dissociate into two adsorbed acetaldehyde units according to

$$D-TiO_2+TiO_2 \rightarrow 2A-TiO_2 \qquad (7)$$

This second case is energetically very advantageous, with ΔE = –65.33 kJ mol^{-1}. There is also loss of entropy due to the stronger surface–acetaldehyde interaction compared to the acetaldehyde–acetaldehyde dimer hydrogen bonding. This difference is, however, overcome by the high gain in energy for the ensuing structure (ΔS = –21.36 J mol^{-1} K^{-1}; ΔG = -60.16 kJ mol^{-1}). Thus we can conclude that—given that there are free available surface sites and that the reaction is not kinetically restricted—the dimer will most likely dissociate to form a second adsorbed acetaldehyde molecule. Thus the adsorbed dimer will turn into a source of acetaldehyde on the surface. We can speculate that, even if multilayer structures are formed instead of an adsorbed dimer, the acetaldehyde–acetaldehyde interactions will be similar. In practice, the formation of such multi-layered structures should follow the inverse of Eqn. (6) and be described as an equilibrium of surface dimers and vapour-phase acetaldehyde.

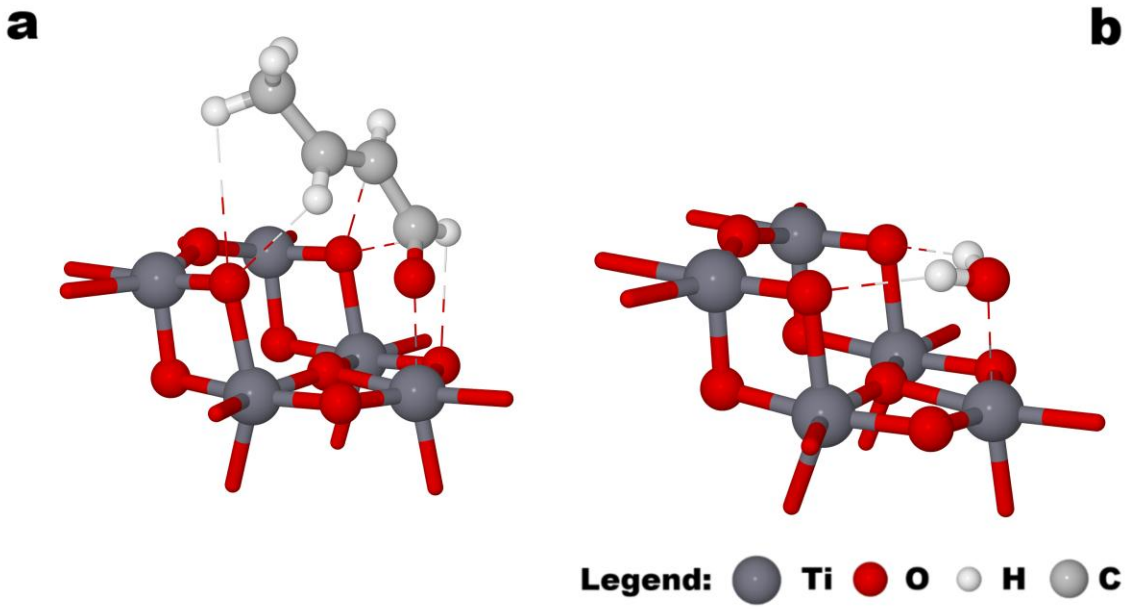

Figure 13. (a) Calculated equilibrium structures of crotonaldehyde, and (b) of water, adsorbed on the anatase (101) surface of a $Ti_5O_{18}H_{16}$ cluster.

We also calculated atomic configurations of adsorbed crotonaldehyde and water, i.e., the

products of the acetaldehyde condensation reaction; optimized structures are shown in Figure 13. The condensation reaction is

$$2CH_3CHO - TiO_2 \rightarrow CH_3(CH)_2CHO - TiO_2 + H_2O\,, \qquad (8)$$

and is predicted to occur spontaneously on the surface with ΔE = –9.24 kJ mol^{-1} and ΔG = –7.79 kJ mol^{-1}. The reaction products are significantly stabilized by the surface (in the gas phase the corresponding values are ΔE = 7.96 kJ mol^{-1} and ΔG = 15.82 kJ mol^{-1}). The predicted ν(C=O) vibration of the adsorbed crotonaldehyde is 1660 cm^{-1}, which clearly is very close to the observed value of 1653 cm^{-1}.

Table 4 Geometric parameters and partial charges for the structures shown in Figures 12 and 13.

		CH_3CHO_{ad} (SI)[§]	$(CH_3CHO)_{2\ ad}$	$CH_3(CH)_2CHO_{ad}$	$H_2O_{\ ad}$
r(O - Ti)		2.190	2.183	2.170	2.318
r(C - O)		1.225	1.231	1.234	
	*		1.213		
r(C H)		1.103	1.101	1.103	
	*		1.114		
r(O···H)		2.299 2.679	2.370 2.743	2.622 2.488	2.235 2.236
	*		2.756 2.767 2.426		
q(O)		-0.385	-0.409	-0.475	-0.660
	*		-0.376		
q(C)		0.351	0.253	0.420	
	*		0.434		
q(Ti)		1.665	1.663	1.706	1.576

(*) Values for the second the dimer unit. Hydrogen bonds marked with an asterisk denote bonding between two units of the adsorbed dimer.

(§) Adsorbate structure SI in Fig. 11.

The binding energy of the surface-adsorbed water was calculated to be ΔE = –93.84 kJ mol^{-1}, which is remarkably close to the reported value ΔE = –88.38 kJ mol^{-1} obtained for the same adsorption

geometry using slab calculations [50], and confirms that the adsorption is a fairly localized process. The corresponding experimental values are reported to be in the range 46–75 kJ mol^{-1} [51], and probably having a large contribution from water that is loosely bonded to surface hydroxyl groups. The binding energy of crotonaldehyde is estimated to be fairly high, ΔE = –82.93 kJ mol^{-1}, which is in qualitative agreement with the temperature programmed desorption (TPD) study by Raskó and Kiss which showed no substantial crotonaldehyde and water desorption below a substrate temperature of 473 K [48]. The same study indicated that acetaldehyde desorbs with a TPD peak maximum at 423 K.

The calculated thermochemical parameters and the calculated and experimentally observed vibrational details for the six considered surface reactions are summarized at Table 3. Selected geometric details and atomic charges are presented in Table 4.

3.3 Generalized kinetic model for acetaldehyde adsorption including dimers

If adsorbed acetaldehyde dimers are added as a source of acetaldehyde according to

$$(CH_3CHO)_2 \rightarrow 2CH_3CHO \rightarrow CH_3(CH)_2CHO + H_2O\,, \tag{9}$$

the kinetic model introduced in Sec. 3.2 can be rewritten as

$$\frac{d\theta_D}{dt} = k_D^{ads}(1.5 - \theta_A - \theta_C - \theta_D) - (k_D + k_D' + k_D^{des})\theta_D\,, \tag{10}$$

$$\frac{d\theta_A}{dt} = k_A^{ads}(1.5 - \theta_A - \theta_C - \theta_D) + 2k_D\theta_D + k_D'\theta_D - k_A^{cond}\theta_A^2\,, \tag{11}$$

$$\frac{d\theta_C}{dt} = \frac{1}{2}k_A^{cond}\theta_A^2\,. \tag{12}$$

The adsorption and condensation terms for acetaldehyde are identical to the ones presented in Sec. 3.2, and the reactions of the dimer species are described through four additional rate constants, with k_D^{ads} being the rate constant for adsorption of the dimer from the gas phase. The fate of the dimer at the surface is described by three rate constants for each of the possible situations: k_D^{des} for desorption back to the gas phase, k_D for dissociation of the dimer into two adsorbed acetaldehyde units, and k_D' for the case where the dimer dissociates with one unit left adsorbed and the second unit returning to the gas

phase. We justify the latter case by the assumption that the interacting unit of the dimer has stronger coupling to the surface than to the second unit (i.e., forming the dimer itself; see Figure 12b). This surmise is confirmed by the DFT calculations.

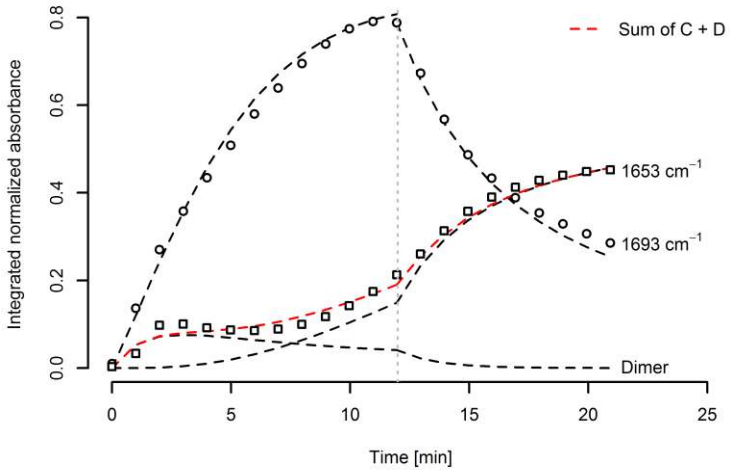

Figure 14. Time-traces of the integrated FTIR absorption bands for acetaldehyde adsorption and condensation on TiO_2. The dashed curves show the results from the generalized model (Eqs. 10-12), which includes acetaldehyde dimer.

The generalized model was fitted to the normalized and integrated spectral data, as reported in Figure 14. Owing to the lack of separate data sets with deconvoluted data for the dimer species (both the dimer and the crotonaldehyde carbonyl bands occur in the same region of the IR spectrum, which prohibits unambiguous deconvolution), the experimental data for crotonaldehyde was fitted with the sum of Eqns. (10) and (12). In principle, this may introduce errors due to different cross-sections of the two species, as discussed in Section 3.1. On the other hand, both species follow the same stoichiometry ratio of 1:2 and 2:1 in their reactions to and from acetaldehyde. It is evident that an inclusion of dimers in the model improves the description of the crotonaldehyde data significantly, and the R^2 factor for the fit increases from 0.81 to 0.97.

Table 5 Calculated rate constants using the simplified (Eqns. 4 and 5), and the generalized (Eqns. 10–12) models, respectively.

		Rate constant (x 10^{-3} s^{-1})			
		without dimer		with dimer	
Reaction	Rate constant notation	Dosing	Purging	Dosing	Purging
$A^{Gas} \rightarrow A^{Ads}$	k^{ads}_{A}	1.82	-	1.4	-
$2A \rightarrow C$	k_A	1.77	4.13	1.26	5.35
$D^{Gas} \rightarrow D^{Ads}$	k^{ads}_{D}	-	-	1.24	-
$D^{Ads} \rightarrow D^{Gas}$	k^{des}_{D}	-	-	3.39	0
$D \rightarrow 2A$	k_D	-	-	4.19	4.49
$D \rightarrow A + A^{Gas}$	k'_D	-	-	4.16	0
R^2 of the fit		0.81		0.97	

Table 5 presents rate constants resulting from both the simple monomer model (Eqns. 4 and 5) and the generalized dimer model (Eqns. 10–12). The introduction of the dimer is seen to produce one significant change, namely a decrease of the acetaldehyde adsorption rate. This decrease is easily explained as a result of the dimer being a second source of acetaldehyde during the dosing. For the dimer itself, the adsorption rate is lower than for the acetaldehyde monomer, which is also supported by the DFT calculations. During dosing, about one third of the dimers is lost and goes back into the gas phase, while the rest of the dimers are reacted—with almost equal possibility—through two dissociation pathways. During purging, when there are no more species present in the gas phase, the energetically favoured dissociation into two adsorbed monomers is preferred. The possibility for each of these reactions is controlled by the amount of available surface sites. During the purging period, the on-going condensation of acetaldehyde vacates surface sites thereby allowing for the all dimers left on the surface to be converted into acetaldehyde.

It is also observed that the rate of acetaldehyde condensation is slow during dosing but increases by a factor two during purging. We believe that there are two effects that contribute to this rate difference: First the condensation rate constant is much higher than the acetaldehyde adsorption constant, so that the adsorption will be a limiting factor and the reaction will be diffusion-controlled and, second, the reaction mechanism may play an important role.

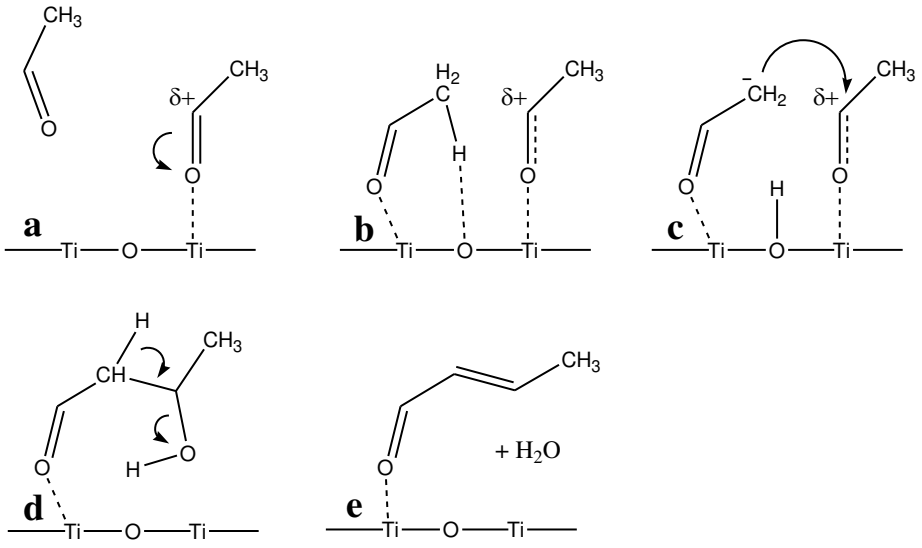

Figure 15. Generalized reaction scheme for acetaldehyde–crotonaldehyde condensation on a TiO_2 surface according to Singh et al. (Ref. 18).

Two adsorbed and activated molecules are required for acetaldehyde condensation to occur, as illustrated in Figure 15. Both of these molecules are coordinated to Ti^{4+} centres, which polarize the carbonyl group and yield additional positive charge on the carbonyl carbon atom. One of the hydrogen atoms in the methyl group of either of the acetaldehyde monomers must interact with surface oxygen. If a proton transfer occurs, this will lead to the formation of a bridge hydroxyl group and a carboanion. Then condensation proceeds first with a nucleophilic attack of the positively charged carbonyl carbon of the second acetaldehyde and then, with another transfer of the proton which was initially transferred to the surface, to the carbonyl oxygen of the attacked acetaldehyde molecule. The two acetaldehyde monomers are now converted into the species 3-hydroxybutanal, which has been identified as short-lived [18], which under atmospheric conditions is quickly converted into crotonaldehyde with release of a water molecule. One should note that this reaction is dependent on the presence of two activated acetaldehyde monomers. However, during the first minute of adsorption when acetaldehyde is present also in the gas phase and the dimers are co-adsorbing, the molecules with dimer configuration will not be reactive. The reason for this inactivity is that a second acetaldehyde unit may shield the carbonyl carbon and thereby stabilize it, as shown in Figure 16. This is also confirmed through the Mulliken population analysis and partial charges, calculated through DFT. The partial charge of the carbonyl carbon of the interacting acetaldehyde unit is decreased, through dimerization, from 0.351 to 0.253 (see Table 4).

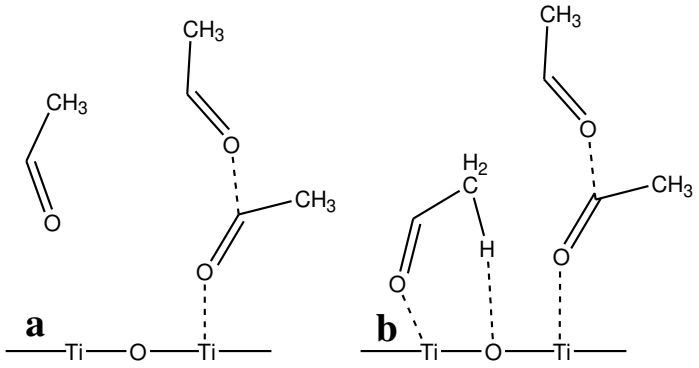

Figure 16. Schematic picture illustrating how the mechanism for acetaldehyde condensation on TiO_2 may be impeded if the carbonyl carbon of the monomer unit is already interacting with the carbonyl group of another acetaldehyde, either from the gas phase or in a dimer structure.

Based on the FTIR data, as well as our DFT calculations we may tentatively conclude that non-covalently bound structures, either dimers or multilayers of acetaldehyde, play a crucial role in the surface reaction kinetics and limit the condensation during gas dosing of the TiO_2 surface. The two processes, i.e. the dissociation and the condensation reaction, would then become self-consistent: the dissociation reaction depends on vacation of more sites, and the condensation reaction depends on the release of an activated acetaldehyde monomers. This double mechanism explains why we observe an increase of the acetaldehyde condensation rate as well as that of the dissociation of the surface adsorbed dimer during the second phase of our experiment.

4. Conclusions

We have investigated the adsorption of acetaldehyde on doctor-bladed TiO_2 anatase films by in situ FTIR spectroscopy and observed condensation of acetaldehyde to crotonaldehyde. Failure to fit mode-resolved FTIR adsorption to a simple acetaldehyde adsorption–condensation reaction led us to the conclusion that a hitherto unknown species, associated with a vibrational mode at 1643 cm^{-1}, should be associated with hydrogen-bonded acetaldehyde dimer species. DFT calculations were used to

predict energies, vibrational spectra, and thermochemical properties of adsorbed acetaldehyde, as well as the most stable hydrogen-bonded dimer and its condensation product, i.e., crotonaldehyde. Good agreement was found between calculated and observed vibrational frequencies.

Our DFT results predict that it is possible for an acetaldehyde dimer to co-adsorb with acetaldehyde monomers. The dimer will then either rapidly decompose into two adsorbed monomer units or dissociate into one adsorbed acetaldehyde with the second fragment desorbed into the gas phase. The former mechanism was predicted to be the energetically favoured. If the number of available adsorption sites is limited, this reaction mechanism is however hindered and adsorbed dimers become a latent acetaldehyde source, which may alter the reaction kinetics when surface sites are liberated. Based on the theoretical predictions we constructed an improved kinetic model, which included acetaldehyde dimers, and which showed excellent agreement with our experimental data.

Acknowledgements

This work was funded by the European Research Council under the European Community's Seventh Framework Program (FP7/2007-2013)/ERC Grant Agreement No. 267234 ("GRINDOOR"). The computations were performed on resources provided by the Swedish National Infrastructure for Computing (SNIC) through Uppsala Multidisciplinary Centre for Advanced Computational Science (UPPMAX) under project p2012120. LÖ is grateful for financial support from the Swedish Research Council (Grant No. VR-2010-3514).

References

[1] W.W. Nazaroff, C.J. Weschler, Atm. Environ. 38 (2004) 2841–2865.

[2] J.-Y. An, S. Kim, H.-J. Kim, J. Seo, Build. Environ. 45 (2010) 1826–1833.

[3] S. Willburn, Am. J. Nursing 99(7) (1999) 71–73.

[4] International Agency for Research on Cancer (IARC), The IARC Monographs Series. Overall Evaluations of Carcinogenicity to Humans, Acetaldehyde [75-07-0] (Vol. 71, 1999), Formaldehyde [50-00-0] (Vol. 88, 2004); http://monographs.iarc.fr/monoeval/grlist.html

[5] European Agency for Safety and Health at Work, European Risk Observatory Report. Exploratory Survey of Occupational Exposure Limits for Carcinogens, Mutagens and Reprotoxic substances at EU Member States Level, 2009; http://osha.europa.eu/en/publications/reports/548OELs/view

[6] Occupational Safety and Health Administration (OSHA). Permissible Exposure Limits. Occupational Safety and Health Administration, Washington, DC (2005);

[7] A. Fujishima, K. Hashimoto, T. Watanabe, TiO_2 Photocatalysis: Fundamentals and Applications, Bkc, Tokyo, 1999.

[8] I. Sopyan, M. Watanabe, S. Murasawa, K. Hashimoto, A. Fujishima, J. Photochem. Photobiol. A: Chem. 98 (1996) 79–86.

[9] E. Obuchi, T. Sakamoto, K. Nakano, F. Shiraishi, Chem. Eng. Sci. 54 (1999) 1525–1530.

[10] H. Hu, W.-J. Xiao, I. Yuan, J.-W. Shi, M.-X. Chen, W.-F. Shang Guan, J. Environ. Sci. 19 (2007) 80–85.

[11] Y. Ohko, D.A. Tryk, K. Hashimoto, A. Fujishima, J. Phys. Chem. B 102 (1998) 2699–2704.

[12] X. Ye, D. Chen, J. Gossage, K. Li, J. Photochem. Photobiol. A: Chem. 183 (2006) 35–40.

[13] M.D. Hernández-Alonso, I. Tejedor-Tejedor, J.M. Coronado, M.A. Anderson, J. Soria, Catal. Today 143 (2009) 364–373.

[14] D.S. Muggli, J.T. McCue, J.L. Falconer, J. Catal. 173 (1998) 470–483.

[15] M.L. Sauer, D.F. Ollis, J. Catal. 158 (1996) 570–582.

[16] R.T. Zehr, M.A. Henderson, Surf. Sci. 602 (2008) 2238–2249.

[17] H. Idriss, M.A. Barteau, Catal. Lett. 40 (1996) 147–153.

[18] M. Singh, N. Zhou, D.K. Paul, K. J. Klabunde, J. Catal. 260 (2008) 371–379.

[19] H. Idriss, C. Diagne, J.P. Hindermann, A. Kiennemann, M.A. Barteau, J. Catal. 155 (1995) 219–237.

[20] V.V. Ordomsky, V.L. Sushkevich, I.I. Ivanova, J. Mol. Catal. A: Chem. 333 (2010) 85–93.

[21] J. Raskó, J. Kiss, Catal. Lett. 101 (2005) 71-77.

[22] J. Rasko, T. Kecskes, J. Kiss, App. Catal. A: General 287 (2005) 244-251.

[23] A.C. Vawdrey, J.L. Oscarson, R.L. Rowley, W.V. Wilding, Fluid Phase Equil. 222–223 (2004) 239–245.

[24] S.W. Milverton, Proc. Roy. Soc. London A 150 (1935) 287–308.

[25] E.A. Alexander, J.D. Lambert, Trans. Faraday Soc. 37 (1941) 421–426.

[26] J.D. Lambert, G.A.H. Roberts, J.S. Rowlinson, V.J. Wilkinson, Proc. Roy. Soc. London A 196 (1949) 113–125.

[27] L.A. Curtiss, M. Blander, Chem. Rev. 88 (1988) 827–841.

[28] C. Guo-Qiang, D. Nan, Acta Phys.-Chim. Sinica 7(3) (1991) 270–275.

[29] K. Tabayashi, M. Chohda, T. Yamanaka, Y. Tsutsumi, O. Takahashi, H. Yoshida, M. Taniguchi, J. Phys.: Conf. Ser. 235 (2010) 012017/1–012017/10.

[30] J.M. Hermida-Ramón, M.A. Ríos, Chem. Phys. Lett. 290 (1998) 431–436.

[31] Z. Topalian, B.I. Stefanov, C.G. Granqvist, L. Österlund, J. Cat 307 (2013) 265-274.

[32] A. Mattson, M. Leideborg, K. Larsson, G. Westin, L. Österlund, J. Phys. Chem. B 110 (2006) 1210–1220.

[33] Z. Topalian, G.A. Niklasson, C.G. Granqvist, L. Österlund, Thin Solid Films 518 (2009) 1341–1344.

[34] R Development Core Team, R: A Language and Environment for Statistical Computing. R Foundation for Statistical Computing, Vienna, Austria, 2011; http://www.R-project.org/

[35] M.W. Schmidt, K.K. Baldridge, J.A. Boatz, S.T. Elbert, M.S. Gordon, J.H. Jensen, S. Koseki, N. Matsunaga, K.A. Nguyen, S.-J. Su, T.L. Windus, M. Dupuis, J.A. Montgomery, Jr., J. Comput. Chem. 14 (1993) 1347–1363.

[36] Y. Zhao, D.G. Truhlar, Theor. Chem. Acc. 120 (2008) 215–241.

[37] Y. Zhao, D.G. Truhlar, Acc. Chem. Res. 41 (2008) 157–167.

[38] M. Horn, C.F. Schwerdtfeger, E.P. Meagher, Z. Kristallogr. 136 (1972) 273–281.

[39] S. Huzinaga (Ed.), Gaussian Basis Sets for Molecular Calculations, Physical Sciences Data 16, Elsevier, Amsterdam, 1984.

[40] P.J. Hay, W.R. Wadt, J. Chem. Phys. 82 (1985) 270–283.

[41] K.L. Schuchardt, B.T. Didier, T. Elsethagen, L. Sun, V. Gurumoorthi, J. Chase, J. Li, T.L. Windus, J. Chem. Inf. Model. 47 (2007) 1045–1052.

[42] R. Ditchfield, W.J. Hehre, J.A. Pople, J. Chem. Phys. 54 (1971) 724–728.

[43] W.J. Hehre, R. Ditchfield, J.A. Pople, J. Chem. Phys. 56 (1972) 2257–2261.

[44] V.A. Rassolov, J.A. Pople, M.A. Ratner, T.L. Windus, J. Chem. Phys. 109 (1998) 1223–1229.

[45] S.F. Boys, F. Bernardi, Mol. Phys. 19 (1970) 553–566.

[46] National Institute of Standards and Technology (NIST), Precomputed Vibrational Scaling Factors; http://cccbdb.nist.gov/vibscalejust.asp

[47] J.E. Rekoske, M.A. Barteau, Langmuir 15 (1999) 2061–2070.

[48] J. Raskó, J. Kiss, Appl. Catal. A: Gen. 287 (2005) 252–260.

[49] W.-C. Wu, S.-J. Yang, C.-H. Ho, Y.-S. Lin, L.-F. Liao, J.-L. Lin, J. Phys. Chem. B 110 (2006) 9627–9631.

[50] Z. Zhao, Z. Li, Z. Zou, Phys. Lett. A 375 (2011) 2939–2945.

[51] T.Z. Srnak, J.A. Dumesic, B.S. Clausen, E. Törnqvist, N.-Y. Topsøe, J. Catal. 135 (1992) 246–262.